Dramatically Comprehensive Improved Electrochemcial Performances of Symmetrical and Asymmetric Supercapacitor under External Magnetic Field

Manying Guo, Zihan Qu, Juan Zhou, Chengdong Han, Xu Liu, Lijun Zhao*

Key Laboratory of Automobile Materials, Ministry of Education and School of Materials Science and Engineering, Jilin University, Changchun, 130022, PR China

*Corresponding authors

E-mail addresses: lijunzhao@jlu.edu.cn (L. Zhao)

2. Experimental Section

2.1. Materials Synthesis

2.1.1 Synthesis of negative material

All chemical agents are commercially available and aren't further purified. MF was built by two NdFeB magnets with the size of 40*20*10 mm, thickness 0.33 mm, basis weight 115 g m^{-2} and resistance 1.89 mΩ cm^2.

Carbon composite was synthesized by a very simple room temperature mixing method. Reduced graphene (rGO), carbon nanotubes (CNTs) and active carbon (AC) dispersed in 100 mL deionized water (DI) were added into a beaker and in a prearranged sequence accompanied by continuous ultrasound for 10 min, and then kept stirring for 1 h. The optimum molar ratio of rGO: CNTs: AC was affirmed as 45: 5: 50 and denoted as GCA. Then, the precipitates were centrifuged and then dried in an oven at 60 ºC for 8 h. Finally, 2 g of GCA was dispersed into 1 L of DI to make 2 g L^{-1} of solution. For other control groups, we adjusted the type and ratio of different carbon materials, such as the pure AC, rGO and AC (1: 1) denoted as GA, and ternary GCA composites with the molar ratio of 25: 5: 70 and 65:5: 30 separately denoted as GCA-70 and GCA-30.

2.1.2 Synthesis of positive material

The NiCoFe/NiCoFe-OH positive material was synthesis in our previous work.[21] NiCoFe precursor was synthesized by a simple grind method at room temperature. Firstly, $NiSO_4 \cdot 6H_2O$ (1.051 g), $CoSO_4 \cdot 7H_2O$ (0.562 g) and $FeSO_4 \cdot 7H_2O$ (0.556 g) were grinded uniformly in a mortar with the molar ratio of 2:1:1. After a certain amount of $NaBH_4$ (0.2 g) was added, the mixture was continuously grinded until the powder turned dark grey. Then the mixed powder was transferred into a beaker. Afterwards, 60 mL of deionized water (DI) was poured into this beaker, causing a violent reaction and producing a large number of bubbles. The precipitates were washed with DI several times, then dispersed in 60 mL DI and sealed in a beaker for 12 h at room temperature. After magnetic separation, the precipitates were dried in an oven at 60 ℃ for 8 h. The resulting product was denoted as NiCoFe/NiCoFe-OH. A certain amount of as-prepared NiCoFe/NiCoFe-OH precursor was dispersed in 25 mL of glycerol and ultrasonicated for 3 min. Then the mixture was transferred into a 50 ml Teflon-lined stainless-steel autoclave. The autoclave was sealed and kept at 200 ℃ for 4 h to gain the NiCoFe/NiCoFe-OH-G composite denoted as NiCoFe/NiCoFe-OH-G4.

2.2. Characterizations

The morphologies of products were investigated using field emission electron microscopy (FESEM, JEOL JSM-6700F) and transmission electron microscopy (TEM, JEOL 2100F). The sample was obtained by N_2 adsorption/desorption isotherms to measure the surface area that was conducted on Micromeritics ASAP 2020 instrument. The high-resolution TEM (HRTEM) was used to measure the crystalline of the samples.

X-ray diffraction (XRD, Rigaku D/Max 2500, Cu Ka radiation: $\lambda= 1.54156$ Å) was used to analyze the crystalline amorphous state and structure. FT-IR spectrometer measurement was conducted using a Nexus 670 FTIR spectrometer (Nexus 670 FTIR spectrometer). X-ray photoelectron spectroscopy (XPS) was used to identify the state of the atom and chemical bond, performed with Al Kα rays on an ESCAlab 220i-XL electronic spectrometer manufactured by VG Scientific. A UV-Visible Spectrophotometer (UV-Vis, Cary 50 Probe) is an analytical instrument based on the principle of ultraviolet-visible spectrophotometry, which utilizes the absorption of radiation in the ultraviolet-visible spectrum region by substance molecules for analysis. Solution wettability was tested using a contact angle meter and interfacial tensiometer (KINO Co, USA) at room temperature (298 K).

2.3. Electrochemical Measurements

The materials were mixed with acetylene black and polyvinylidene fluoride (PVDF) in a mass ratio of 8: 1: 1 in a proper amount of N-methylpyrrolidone (NMP) solution and deposited in carbon cloth substrates. The as-prepared electrodes were dried overnight at 80 °C for 8 h in the vacuum. The mass loadings for both GCA and NiCoFe/NiCoFe-OH active materials on carbon cloth substrates are in the range of 1–2 mg cm^{-2}. The electrochemical measurements of working electrodes (GCA and NiCoFe/NiCoFe-OH) were tested using a three-electrode system with a platinum foil counter electrode and a silver chloride (Ag/AgCl) reference electrode at room temperature. The electrolyte used a 3.0 mol L^{-1} KOH aqueous solution. To test the electrochemical properties of electrode materials in a magnetic field, the whole

electrochemical system was fixed between two magnets of the same sizes.

3. Electrochemical Calculations

The specific capacitance (C) of an individual electrode, SSA and ASC device could be attained based on Equ. (1):

$$C = I\Delta t/(mV) \tag{1}$$

Wherein C, I, Δt and m represent the specific capacitance (F g^{-1}), current (A), discharge time (s) and the total active materials mass (g) of an individual electrode or ASC device, V is behalf on the voltage of individual electrode, SSA and ASC.

The matching mass of positive and negative electrodes is obtained according to Equ. (2):

$$m^+/m^- = C^- V^-/(C^+ V^+) \tag{2}$$

wherein m^+ and m^- correspond to the mass of the active material (g) of positive and negative electrodes; C^+ and C^- are the specific capacitance (F g^{-1}) of positive and negative electrodes; V^+ and V^- are the voltage of specific capacitance of positive and negative electrodes.

For ASC devices, the energy density (E, W h kg-1) and power density (P, W kg-1) are available based on Equ. (3) and Equ. (4):

$$E = I\int V \, dt/3.6 \, (m^+ + m^-) \tag{3}$$

The constant 3.6 was adopted when the energy density (E) is in W h kg^{-1}, the current (I) is in mA, the voltage (V) is in V, the time (t) is in seconds, and the mass (m) is in mg. The mass used in the calculation for the hybrid supercapacitor device was based on the total mass of positive and negative composite.

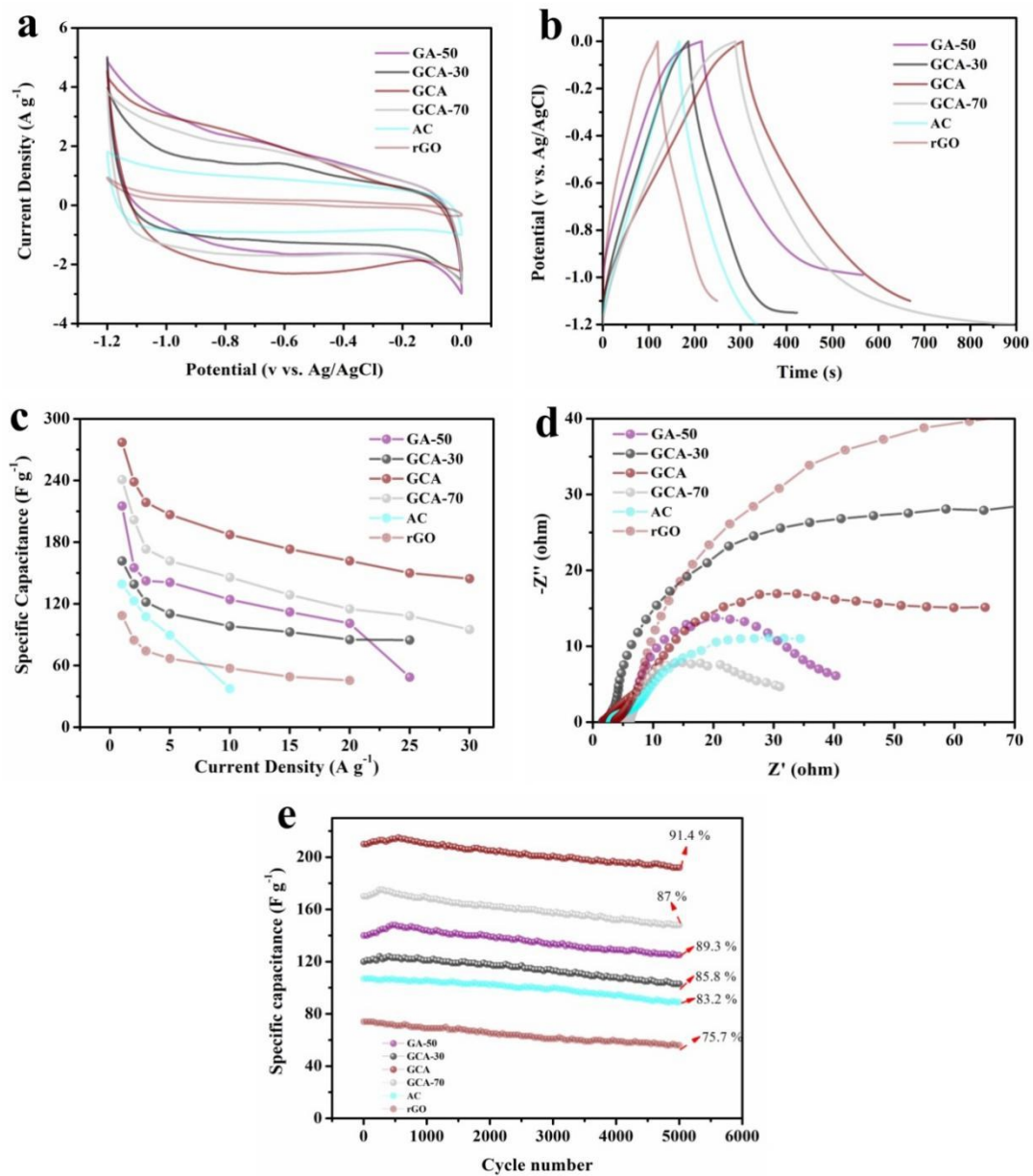The power density (W kg^{-1}) was calculated using the following equation:

$$P = E/\Delta t \tag{4}$$
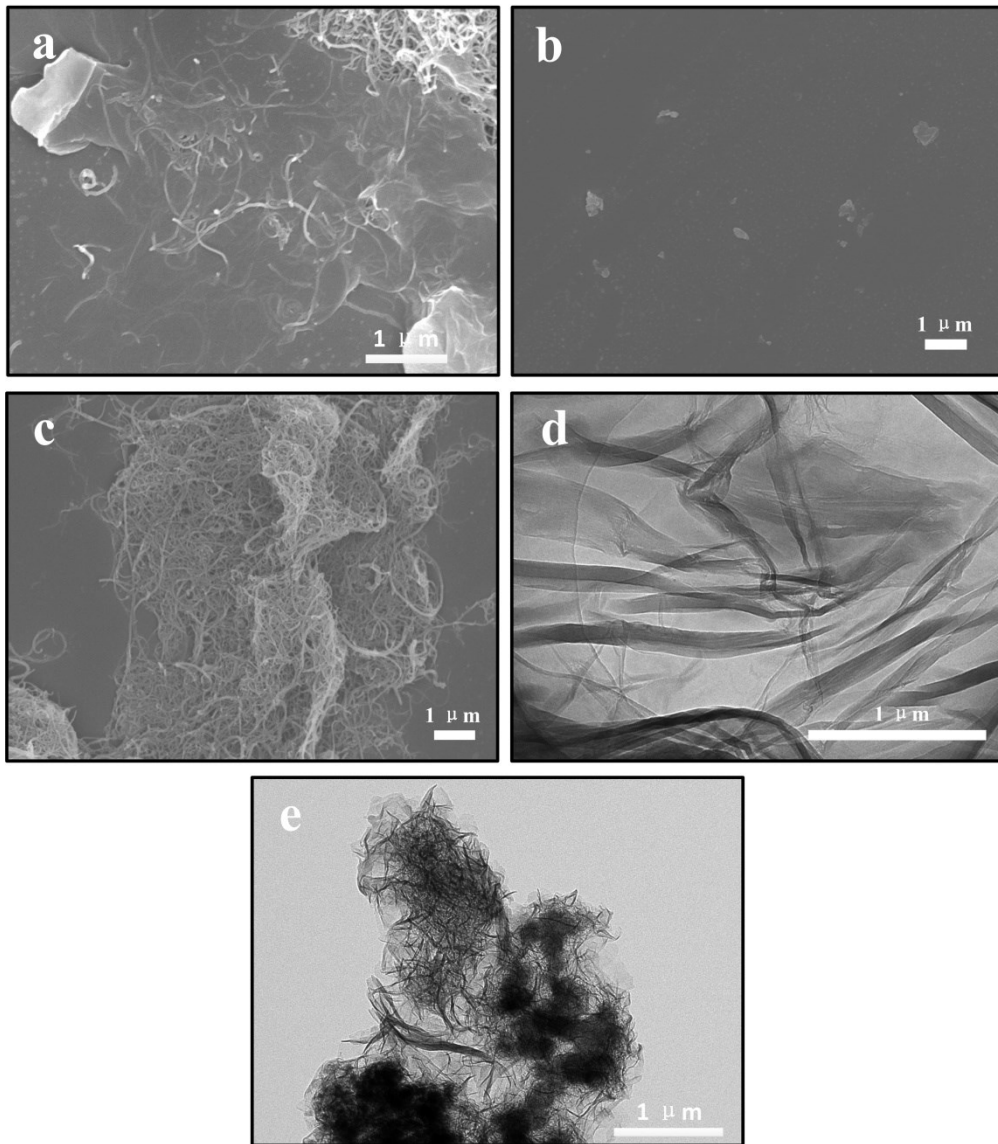
Fig. S1. (a) GCA, (b) AC and (c) CNTs SEM images, TEM images of (d) rGO, and (e) NiCoFe/NiCoFe-OH.
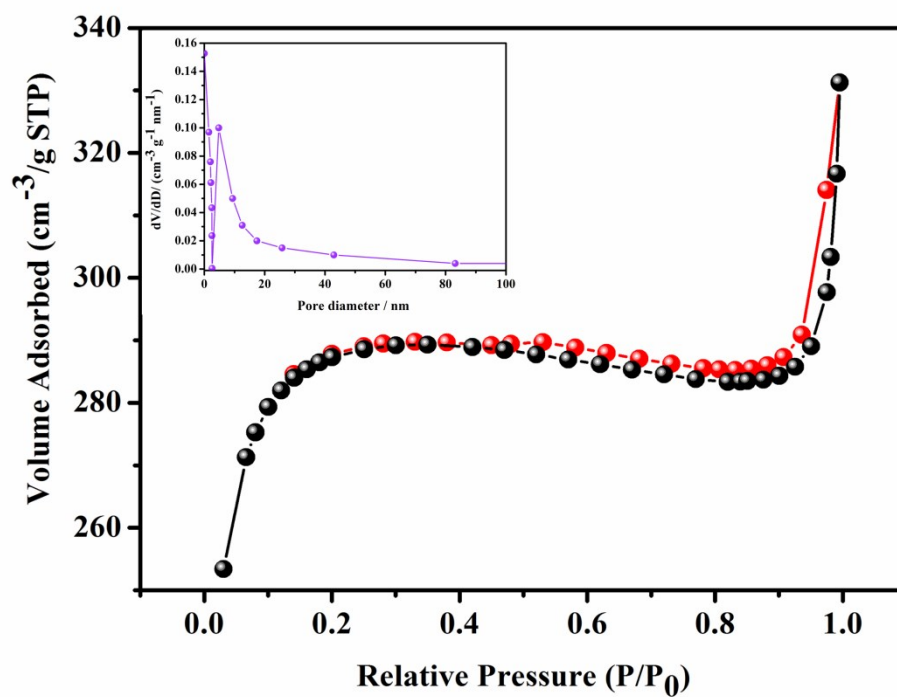
Fig. S2. BET surface area of GCD composite; insets showing its corresponding BJH pore-size distribution graphs.

Fig. S3. (a) CV curves of the AC, rGO and GCA composites measured at the scan rate of 10 mV s^{-1}, (b) GCD profiles at 1 A g^{-1}, (c) Specific capacitances and rate performance at different current densities, (d) Nyquist plots, (e) Cycling stability at 3 A g^{-1}.
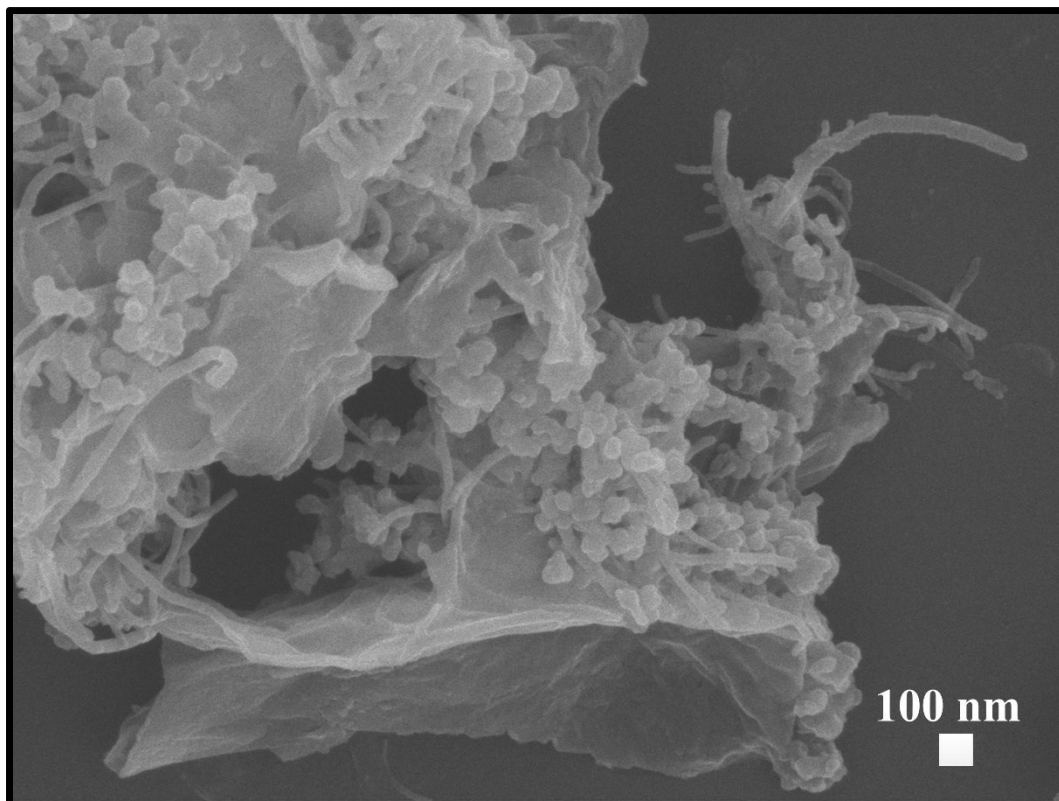
Fig. S4. SEM image of GCA after 5000 cycles.
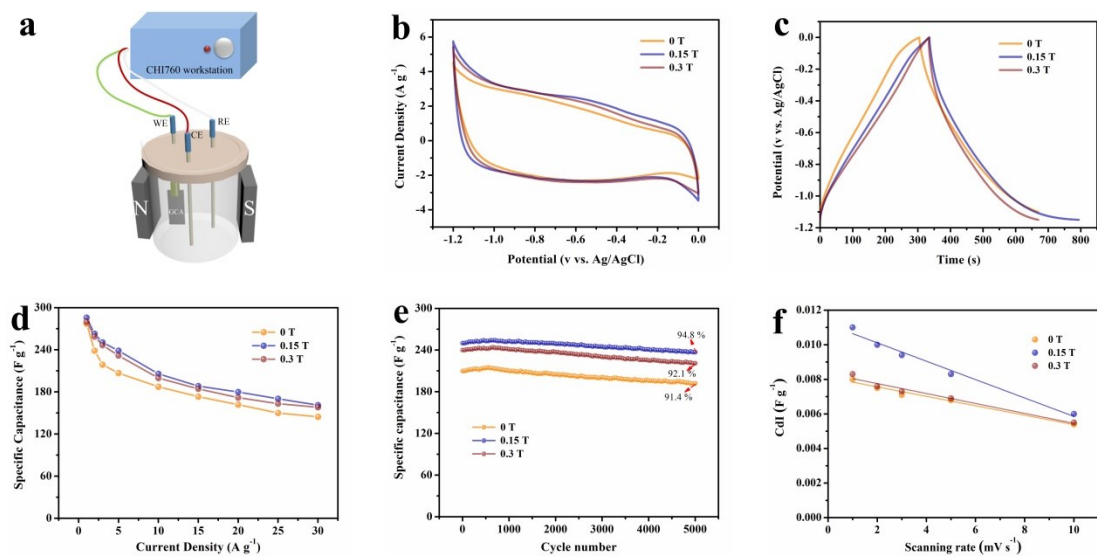
Fig. S5. (a) Schematic illustration of GCA composite test in a three-electrode system with an MF, (b) CV curves at the scan rate of 10 mV s^{-1}, (c) GCD profiles at 1 A g^{-1}, (d) specific capacitances and rate performance at different current densities, (e) cycling stability at 3 A g^{-1} of GCA at 0, 0.15 and 0.3 T, (f) electrochemical double-layer capacitances of GCA under different magnetic fields.
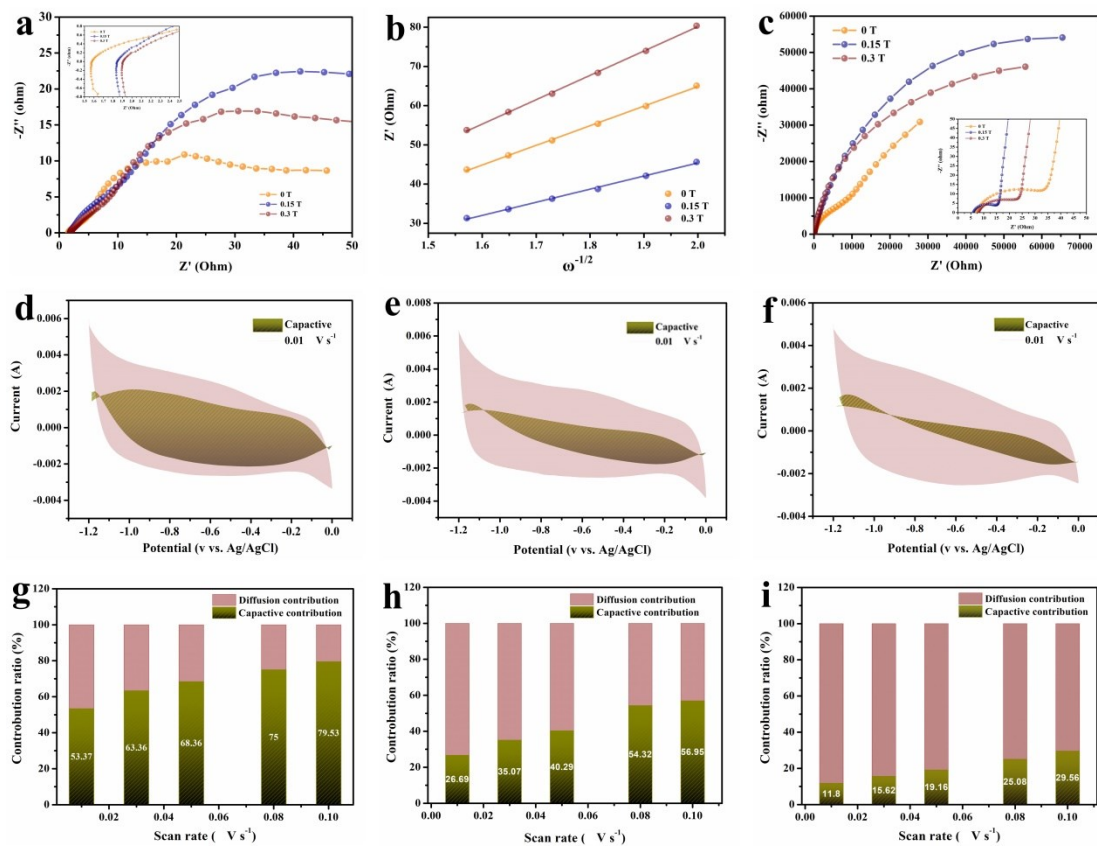
Fig. S6. (a) Nyquist plots (inset: the magnified of Nyquist plots), (b) Z'- $\omega^{-1/2}$ plots of GCA, (c) Nyquist plots (inset: the magnified of Nyquist plots) of KOH electrolyte, (d-f) Capacitive contribution (colored area) at a scan rate of 0.01 V s^{-1}, (g-i) Normalized contribution ratio of capacities at different scan rates.
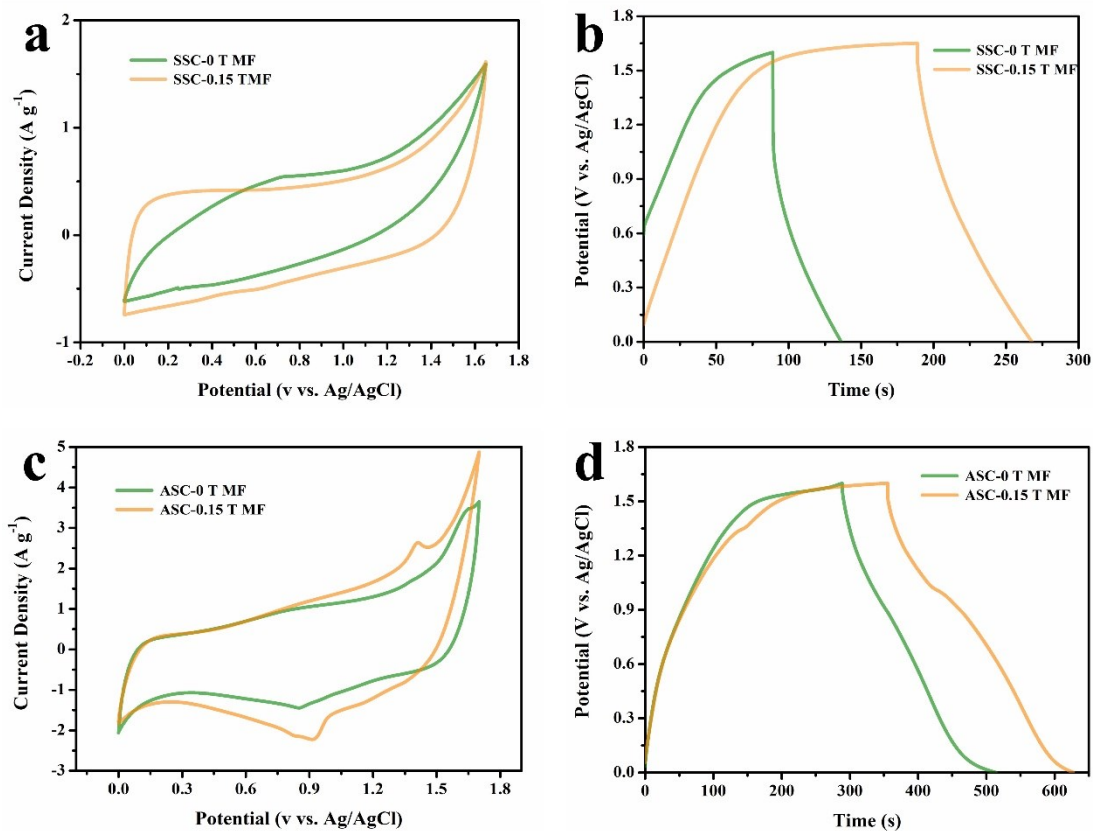
Fig. S7. (a, c) CV curves at a 10 mV s⁻¹ of scan rate, (b, d) GCD profile at 1 A g⁻¹ of SSC and ASC.
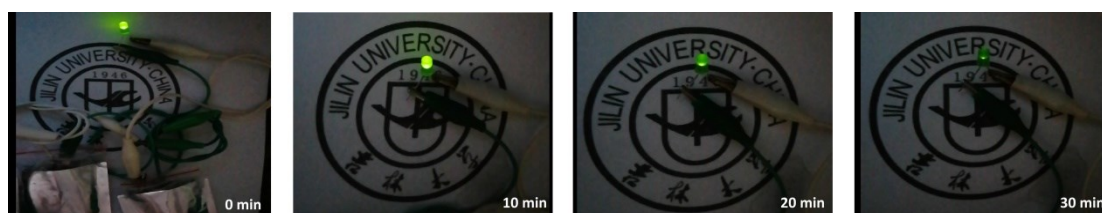
Fig. S8. The practical application of ASC-0.15 T MF in lighting green bubble.
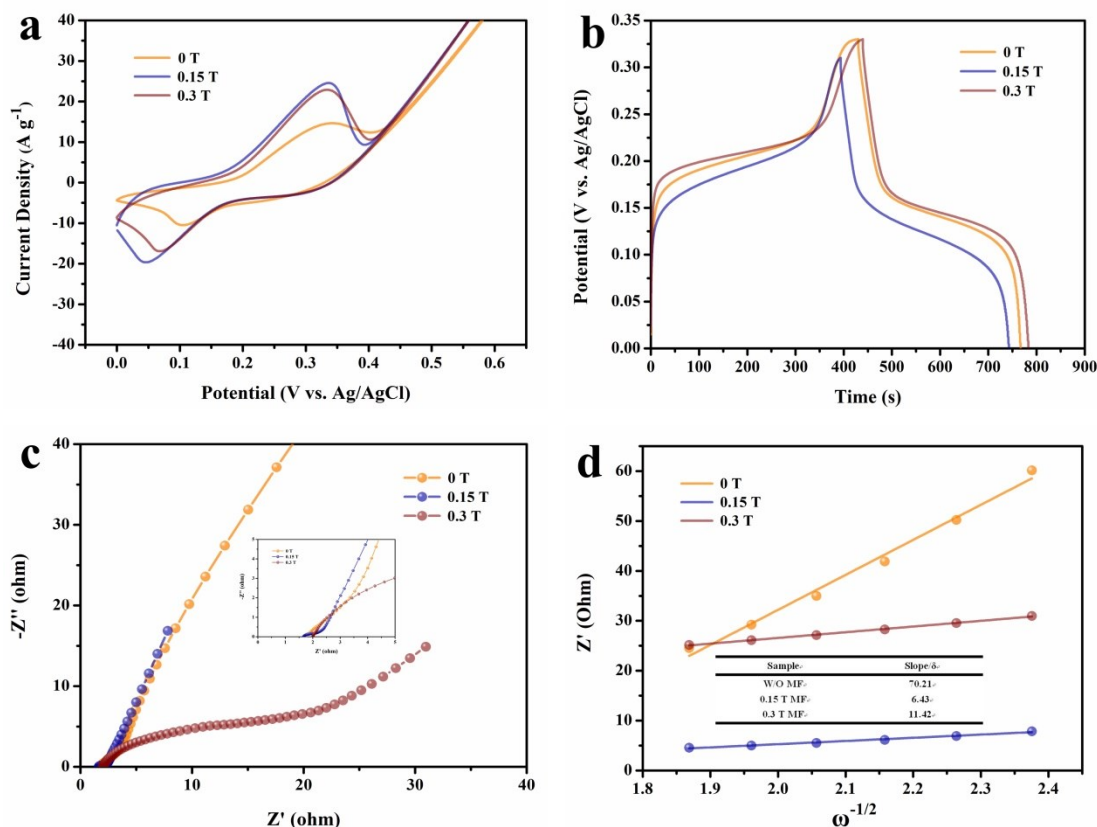
Fig. S9. (a) CV curve at scanning rate 10 mV s^{-1} with potential from 0-0.6 V, (b) GCD profiles at 1 A g^{-1}, (c) Nyquist plots, (d) Relationship between Z_{re} and $\omega^{-1/2}$ in the low-frequency region of NiCoFe/NiCoFe-OH cathode with different MF strengths.

For having better electrochemical properties of ASC, the cathode material is also important. We use the solid-state-grinding method synthesized 3D hybrid architecture NiCoFe/NiCoFe-OH as cathode, which has reported in our previous works. It has a larger CV curve area and the calculated specific capacitance achieves 1018.2 F g^{-1} at 1 A g^{-1} with the 2.07 Ω Rct value. To evaluate the influence of MF on the electrochemical performance of NiCoFe/NiCoFe-OH as cathode, we tested CV, GCD and EIS properties by employing 0.15 T and 0.3 T MF. The specific capacitances and are 1122.6 F g^{-1} and 1039.4 F g^{-1} at 1 A g^{-1} with 1.73 Ω and 1.85 Ω Rct value under 0.15 T and 0.3 T MF, respectively.

Table 1 Comparison of the specific capacitance, energy density, power density and cycle stability of the reported symmetric supercapacitor of carbon materials to our work.

	Specific Capacitance (F g^{-1})	Energy Density (Wh kg^{-1})	Power Density (W kg^{-1})	Cycle Stability
CS/His-B//CS/His-B[35]	58.9 (0.5 A g^{-1})	30.1	225.1	100% (100000 at 2.5 A g^{-1})
MGHG//MGHG[36]	64 (0.5 A g^{-1})	30	1000	88% (8500 at 5 A g^{-1})
p-RGO-5//p-RGO-5[37]	29.99 (1 A g^{-1})	24.67	400	94.98% (10000 at 1 A g^{-1})
MB@3D-rGO//MB@3D-rGO[38]	59.04 (0.5 A g^{-1})	8.2	248.9	81%(10000 at 50 mV s^{-1})
BNC-20// BNC-20[39]	157 (1 A g^{-1})	9.33	400	91% (10000, at 1 A g^{-1})
PM6//PM6[40]	137.7 (1 A g^{-1})	9.345	687	95.4% (3000 at 1 A g^{-1})
KNOSC//KNOSC[41]	91.8 (1 A g^{-1})	15.4	550	//
NPCF//NPCF[42]	46.2 (1 A g^{-1})	20.77	450	99.11% (5000 at 10 A g^{-1})
N-CNT@CF//N-CNT@CF[43]	155 (0.5 A g^{-1})	5.5	254	93% (10000 at 10 A g^{-1})
3DAC-20//3DAC-20[44]	157 (0.5 A g^{-1})	37.6	7100	94% (7000 at 1 A g^{-1})

This work	31.4 (0 T)/47.8 (0.15 T)	11.2/18.1	861.6/889	72.8%/90.5 (20000 at 3 A g^{-1})	

Table 2 Summarized SSC and ASC electrochemical performances with 0 T and 0.15 T MF.

SSC	Specific Capacitance （F g^{-1}）	Rate Performance (1-10 A g^{-1})	Energy Density (Wh kg^{-1})	Power Density (W kg^{-1})	Cycle Stability (after 20 k)	Self-discharge (24 h)
SSC-0.15 T MF	47.8	45.2 %	18.1 / 8.2	889 / 8430.3	90.5 %	0.365 V
SSC-0 T MF	31.4	38.2 %	11.2 / 4.3	861.6 / 8113.2	72.8 %	0.32 V
SSC-0.3 T MF	39.1	44.1 %	14.7 / 6.5	850 / 7900.3	85.6 %	0.343 V
ASC	Specific Capacitance （F g^{-1}）	Rate Performance (1-10 A g^{-1})	Energy Density (Wh kg^{-1})	Power Density (W kg^{-1})	Cycle Stability (after 20 k)	Self-discharge (24 h)
ASC-0.15 T MF	170.7	46.4 %	61.4 / 28.5	974.6/ 8142.8	92.7 %	0.53 V
ASC-0 T MF	142.3	45.2 %	50.6 / 24	812.2 / 8000	91.5 %	0.49 V
ASC-0.3 T MF	158.6	50.1 %	59.9 / 29.9	820.5 / 8262.7	92.1 %	0.51 V

References

35 L. Yang, D. L. Wu, T. Wang, D. Z. Jia, *ACS Appl. Mater. Interfaces,* 2020, **2**, 18692−18704.

36 N. Ahmed, A. Amer, B. A. Ali, A. H. Biby, Y. I. Mesbah, N. K. Allam, *Sustain. Mater. Techno.,* 2020, **25**, e00206.

37 P. Li, H. P. Li, X. L. Zhang, X. C. Zheng, *J. Energy Storage,* 2021, **33**, 102044.

38 X. P. Zhou, T. Meng, F. Y. Yi, D. Shu, D. M. Han, Z. H. Zhu, A. M. Gao, C. Liu, X. Li, K. M. Yang, H. Yi, *J. Power Sources,* 2020, **475**, 228554.

39 L. Luo, Y. L. Zhou, W. Yan, X. Wu, S. R. Wang, W. G. Zhao, *Electrochim. Acta,* 2020, **360**, 137010.

40 F. Regan Maria Sundar Raj, N. Victor Jaya, G. Boopathi, D. Kalpana, A. Pandurangan, *Mater. Chem. Phys.,* 2020, **240**, 122151.

41 H. R. Peng, B. Yao, X. J. Wei, T. Y. Liu, T. Y. Kou, P. Xiao, Y. H. Zhang, Y. Li, *Adv. Energy Mater.,* 2019, **9**, 1803665.

42 L. Lin, H. M. Xie, Y. Lei, R. Z. Li, X. Y. Liu, J. K. Ou, *J. Mater. Sci. Mater. Electron.,* 2020*,* **31**, 10825-10835.

43 Thapelo P. Mofokeng, Zikhona N. Tetana, Kenneth I. Ozoemena, *Carbon,* 2020, **169**, 312-326.

44 N. Jabeen, A. Hussain, Q. Y. Xia, S. Sun, J. W. Zhu, H. Xia, *Adv. Mater.,* 2017, **29**, 1700804.